Solution-Phase, Triangular Ag Nanotriangles Fabricated by Nanosphere Lithography

Amanda J. Haes,[†,§] Jing Zhao,[†] Shengli Zou,[†] Christopher S. Own,[‡] Laurence D. Marks,[‡] George C. Schatz,*[,†] and Richard P. Van Duyne*[,†]

Department of Chemistry, Northwestern University, 2145 Sheridan Road, Evanston, Illinois 60208-3113, and Department of Materials Science and Engineering, Northwestern University, 2220 North Campus Drive, Cook Hall No. 2036, Evanston, Illinois 60208-3108

Received: March 7, 2005; In Final Form: April 17, 2005

A novel method to produce solution-phase triangular silver nanoparticles is presented. Ag nanoparticles are prepared by nanosphere lithography and are subsequently released into solution. The resulting nanoparticles are asymmetrically functionalized to produce either single isolated nanoparticles or dimer pairs. The structural and optical properties of Ag nanoparticles have been characterized. Mie theory and the Discrete Dipole Approximation method (DDA) have been used to model and interpret the optical properties of the released Ag nanoparticles.

Introduction

Advances in the field of nanoparticle optics allow for a deeper understanding of the relationship between material properties such as composition, size, shape, and local dielectric environment and their observed optical properties. An understanding of these properties holds both fundamental and practical significance. From a fundamental perspective, it is important to systematically explore how nanoscale structural and local environmental factors cause optical property variations. The most important optical excitations in noble metal nanoparticles arise from localized surface plasmon resonances (LSPR), which are collective oscillations of the conduction electrons of the individual nanoparticles.[1−9] LSPR excitation allows the optical properties of these nanoparticles to be monitored with UV−vis spectroscopy and it makes possible a variety of surface-enhanced spectroscopies. Many aspects of LSPR excitation can be described accurately with classical electromagnetic theory, which makes possible the use of theory to guide in the design of nanoparticle systems which deliver optimal response. From a practical perspective, the tunable optical properties of nanostructures make it possible to use these materials in surface-enhanced spectroscopy,[10−14] optical filters,[15,16] plasmonic devices,[17−20] and sensors.[21−35]

Until recently, there were only limited methods for the synthesis of monodisperse, nonspherical noble metal nanoparticles, which meant that the practical applications of these particles were limited. Recent advances in controlled syntheses of spheres,[36,37] rods, [38−40] triangular prisms,[41−43] disks,[44−46] cubes,[47] and branched nanocrystals[48] have improved both the fundamental understanding and practical use of these nanoparticles for sensing and spectroscopic devices.

Traditionally, the synthesis of noble metal nanoparticles relies on the ability to reduce a metal salt in a controlled environment.[49−53] An alternative to solution-phase nanoparticle synthesis is nanoparticle fabrication on solid substrates. A standard lithographic approach for fabricating surface-confined nanoparticles is electron beam lithography (EBL). This approach is effective at fabricating large arrays of template-defined nanoparticle structures. While EBL provides exquisite control over nanoscale morphology, it is expensive and time-consuming.

Nanosphere lithography (NSL) is a powerful fabrication technique that inexpensively produces surface-confined nanoparticle arrays with controlled shape, size, and interparticle spacing.[54] NSL begins with the self-assembly of size-monodisperse nanospheres of diameter D into a two-dimensional colloidal crystal.[54−56] As the solvent of the nanosphere solution evaporates, capillary forces draw the nanospheres together thereby crystallizing them into a hexagonally close-packed pattern on the substrate. Following self-assembly of the nanosphere mask, a metal or other material is deposited onto the nanosphere-coated substrate. After metal deposition, the nanosphere mask is removed via sonication in ethanol resulting in surfaced-confined nanoparticles with triangular footprints.

In previous studies, it was reported that nanoparticle adhesion to glass is weak; that is, less than 10 nN (normal force) is required for delamination.[29] Here, we take advantage of this property to purposefully remove the nanoparticles from the substrate. Because NSL can be used to fabricate monodisperse triangular nanoparticles and because nanoparticle adhesion to glass is poor, the methods developed here can be used to make monodisperse nanoparticles in solution. To prevent nanoparticle aggregation, the nanoparticles must be functionalized with a stabilizing molecule prior to their release. While several molecules were considered (citrate, 11-mercaptoundecanoic acid, hexanethiol), hexadecanethiol provided the largest degree of nanoparticle stabilization.

Experimental Section

First, NSL was used to create monodisperse, surface-confined Ag nanotriangles.[21,28] Polystyrene nanospheres (∼2 μL, diameter = 400 nm ± 7 nm, Interfacial Dynamics) were drop-coated onto piranha cleaned and base treated glass substrates[21] (Fisher) and were allowed to dry, forming hexagonal close-packed monolayer of spheres, which served as a deposition mask. The samples were mounted into a Consolidated Vacuum Corporation vapor deposition chamber. A Leybold Inficon XTM/2 quartz crystal microbalance was used to monitor the thickness of the

* Address correspondence to these authors. R.P.V.D.: e-mail vanduyne@chem.northwestern.edu, phone (847) 491-3516, fax (847) 491-7713. G.C.S.: e-mail schatz@chem.northwestern.edu, phone (847) 491-5657, fax (847) 491-7713.

† Department of Chemistry, Northwestern University.

§ Current address: Naval Research Laboratory, Washington D.C.

‡ Department of Materials Science and Engineering, Northwestern University.

10.1021/jp051178g CCC: $30.25
Published on Web 05/14/2005

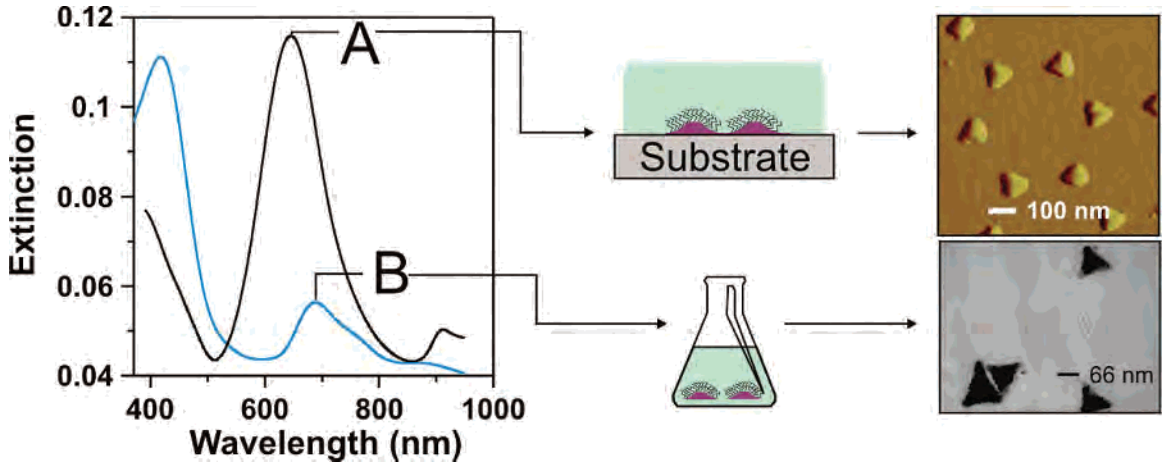

Figure 1. Fabrication, optical characterization, and structural characterization of released Ag nanoparticles (a = 100 nm, b = 50 nm Ag). (A) Ag nanoparticles are first fabricated via NSL on glass substrates. A representative LSPR spectrum of hexadecanethiol-functionalized nanoparticles in ethanol has an extinction maximum located at 645.6 nm. AFM reveals average nanoparticle heights of 52 nm and widths of 100 nm. (B) Upon dislodging the nanoparticles from the glass substrate into bulk ethanol, a representative LSPR spectrum has two maxima located at 417.9 and 682.1 nm. TEM reveals nanoparticles with in-plane widths of ~95 nm.

metal being deposited. Ag (D. F. Goldsmith) was evaporated onto the samples to a fixed thickness of 50 nm. Following metal deposition, the samples were sonicated for 3−5 min in ethanol (Pharmco) to remove the polystyrene nanosphere mask, creating ordered arrays of Ag nanoparticles on glass substrates. Atomic force microscope (AFM) images were collected with a Digital Instruments Nanoscope IV microscope and Nanoscope IIIa controller operating in tapping mode. Transmission electron microscope (TEM) images were collected with a Hitachi 8100 TEM.

The extinction maximum, λ_{max}, of each sample was monitored and recorded with a UV−vis spectrometer. Macroscale UV−vis extinction measurements were collected with an Ocean Optics (Dunedin, FL) SD2000 fiber optically coupled spectrometer with a CCD detector. All spectra in this study are macroscopic measurements performed in standard transmission geometry with unpolarized light. Solution-phase measurements were collected in quartz cuvettes (path length = 1 cm). The white light probe beam diameter was approximately 2 mm. The extinction maximum of each spectrum was located by calculating its first derivative.

Results and Discussion

Although several sphere sizes and materials were used for metal depositions, only spheres with D = 400 nm and metal thicknesses d_m = 50 nm of Ag have been included in our studies of particle removal from the substrate. While expected variations in the nanoparticles' optical properties and size were observed in the preliminary data, similar observations were made. For this reason, representative results from a single sphere size are included here. For these experiments, the samples were placed in 1 mM hexadecanethiol (in ethanol) for 48−96 h, immediately after the above-mentioned sonication step. After thorough rinsing, the samples were filtered with 400 nm filters (GE Osmonics, Inc. Minnetonka, MN) to remove large particles arising from defects in the nanosphere mask and were subsequently analyzed with UV−vis spectroscopy. A representative LSPR spectrum of surface-confined Ag nanoparticles that are coated in a self-assembled monolayer (SAM) of hexadecanethiol and immersed in ethanol is displayed in Figure 1A. AFM reveals nanoparticles with average heights of 52 nm and perpendicular bisectors of ~100 nm.

To create a solution that has an equivalent concentration of nanoparticles to that in Figure 1A, five samples (D (sphere diameter) = 400 nm, b (nanoparticle height) = 50 nm Ag) which have been functionalized with hexadecanethiol were used. Following SAM incubation, the samples are rinsed thoroughly in ethanol and the nanoparticles are sonicated off the substrate in 5 mL of neat ethanol. The UV−vis spectra and structures of hexadecanethiol functionalized Ag nanoparticles on a substrate and in solution are compared in Figure 1, parts A and B, respectively. Upon release, the LSPR spectrum of the nanoparticles changes dramatically, resulting in an intense peak at 418 nm and a weak broad peak centered at 682 nm.

Because of this drastic change in optical properties, it was important to investigate the morphology of the solution-phase nanoparticles. To obtain information regarding nanoparticle structure, the released nanoparticles were imaged in the transmission electron microscope (TEM). As revealed in Figure 2A, the nanoparticles retain their triangular shape and have perpendicular bisectors of ~95 nm. This is the first time that nanoparticles fabricated via NSL have been structurally characterized with TEM. As shown in Figure 1A, when analyzed with AFM, the nanoparticles were revealed to have perpendicular bisectors of ~100 nm.[1] Additionally, the edges of the nanoparticles were straight. When analyzed with TEM, new and more precise details are revealed. First, the nanoparticle dimensions are in closer agreement to geometrically predicted dimensions than what is revealed through AFM. Furthermore, the geometrical shape, which is cusped triangular edges, is clearly seen with TEM. Upon closer examination of the TEM images, a large number of smaller (less than 10 nm), seemingly spherical nanoparticles were observed throughout the nanoparticle samples (Figure 2B, red circles). These small features likely arise from larger nanoparticles breaking up during sample sonication in the release step. Not only can the structure of nanoparticles be analyzed with TEM, but their crystallinity can also be determined with diffraction. Because these nanoparticles are fabricated on glass, the nanoparticles are not expected to be single crystals, and indeed, in Figure 2C, the diffraction pattern confirms that the nanoparticles are polycrystalline but with small crystalline domains. We anticipate that if the Ag nanoparticles were grown epitaxially on an atomically flat surface such as mica that they would be nanocrystals.

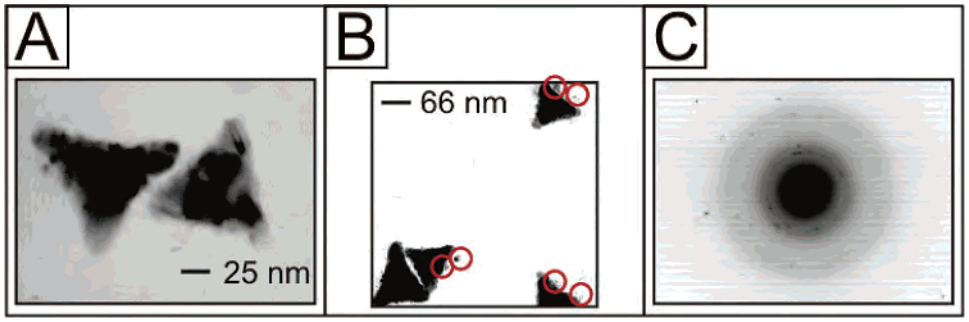

Figure 2. TEM characterization of released Ag nanoparticles. (A) Representative Ag nanoparticles are triangular and have in-plane widths of ~95 nm. (B) In addition to triangular particles, small spherical nanoparticles (red circles), average diameter = 10−20 nm, are revealed in each sample. (C) TEM diffraction reveals the polycrystalline nature of the nanoparticles.

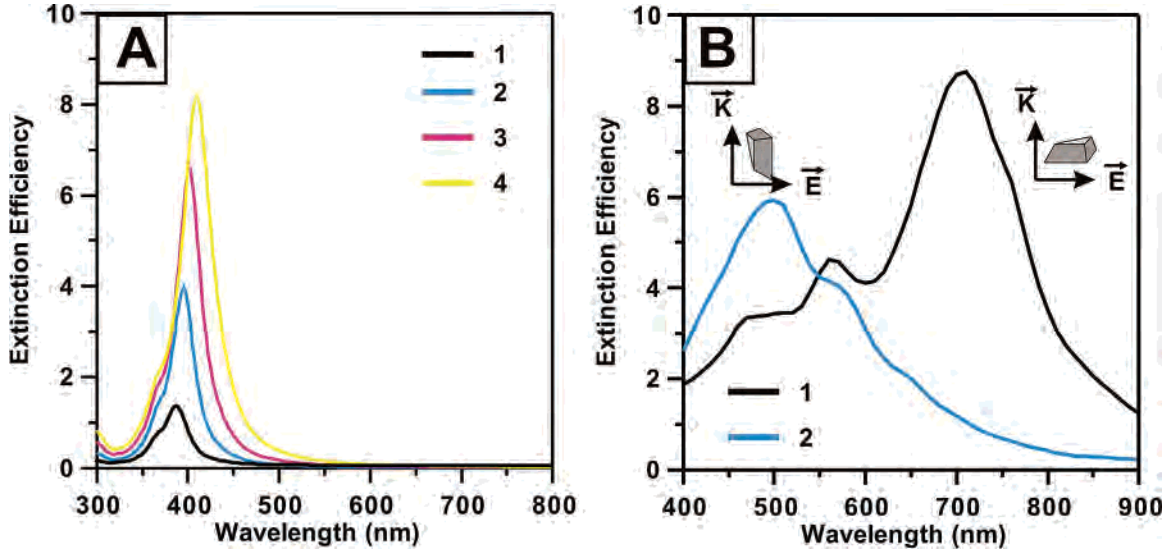

Figure 3. Theoretical calculations for released nanoparticles. (A) Mie theory calculations of the extinction spectra of a small Ag nanosphere with a full monolayer of 1-hexadecanethiol (n = 1.45, layer thickness = 2.6 nm) that is immersed in ethanol. The sphere radii were chosen to be (1) 5, (2) 10, (3) 15, and (4) 20 nm. (B) DDA calculations of the extinction spectra of Ag nanoparticles (a = 95 nm, b = 50 nm) with a SAM shell of 1-hexadecanethiol (n = 1.45, layer thickness = 2.0 nm) in ethanol (n = 1.36). (1) In-plane polarization and (2) out-of-plane polarization of the released Ag nanoparticles.

As revealed in the TEM images in Figure 2, there are two primary types of nanoparticles found in the released nanoparticle samples: (1) small spherical Ag fragments and (2) truncated tetrahedral Ag nanoparticles that are similar to what is produced on the substrate. Both structures may influence the optical spectrum of the released nanoparticles observed in Figure 1B. To model these experimental results, Mie theory[57,58] and Discrete Dipole Approximation (DDA)[59,60] calculations have been used to simulate the spherical and truncated tetrahedral nanoparticles, respectively. All calculations refer to silver nanoparticles with a dielectric constant taken from Lynch and Hunter.[61] The surrounding medium in all calculations is ethanol (refractive index of 1.36). The refractive index of hexadecanethiol is taken as 1.45.

Mie theory, the exact analytical solution of Maxwell's equations for a sphere, has been used to model hexadecanethiol-coated Ag nanospheres with radii ranging from 5, 10, 15, and 20 nm. Figure 3A shows that as the sphere radius increases, the LSPR extinction maximum increases from ~390 nm to 410 nm. This maximum agrees well with the "blue" peak observed in the experimental results as seen in Figure 1B.

DDA, a numerical method suitable for modeling nanoparticles with different sizes and shapes, is suitable to calculate the optical spectra of triangular nanoparticles by representing them as a cubic lattice of polarized points. The number of polarized points is determined by the dimension of the object and the chosen grid spacing. In these studies, the object is modeled as a simple truncated tetrahedron that is isolated in a fixed dielectric environment. The calculations are performed with the following parameters: a = 95 nm (in-plane diameter), b = 50 nm (out-of-plane height), and DDA grid spacing = 2 nm. Our past work with these calculations has demonstrated that this choice of parameters will produce extinction spectra that are adequately converged for what we need in this study.

Figure 3B presents the in-plane (Figure 3B-1) and out-of-plane (Figure 3B-2) polarized spectra of a single Ag truncated tetrahedron (immersed in ethanol with a hexadecanethiol monolayer). The in-plane polarization, in which the polarization vector, $\vec{E}$, of the incident light is parallel to the triangular surface and the wavevector, $\vec{K}$, is perpendicular, has a maximum that is located at ~710 nm. The out-of-plane polarization, in which $\vec{E}$ of the incident light is perpendicular to the triangular surface, has a local extinction maximum located at ~500 nm.

In comparison to the experimental results (Figure 1B), the calculated in-plane polarized spectrum (Figure 3B-1) corresponds to the red peak in Figure 1B and the out-of-plane polarization peak corresponds to the blue experimental maximum. Considering the theoretical results from both the Mie and DDA models, we may conclude that the intense local maximum centered at ~420 nm (experimental) arises from the combined effect from the absorption of small spherical nanoparticles and the out-of-plane polarization of truncated tetrahedral nanoparticles.

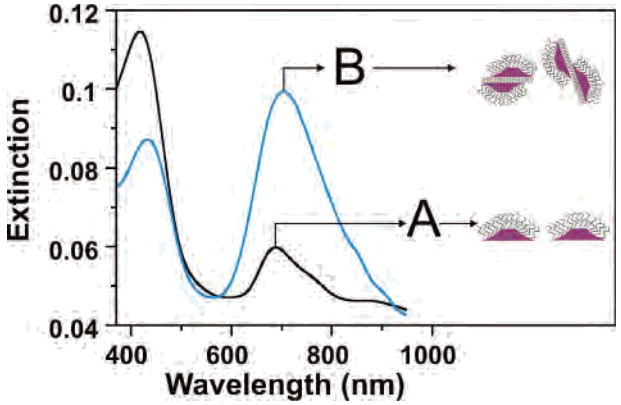

Figure 4. Demonstration of asymmetric functionalization of released nanoparticles. LSPR spectrum of Ag nanoparticles (A) before ($\lambda_{max,1}$ = 417.9 nm and $\lambda_{max,2}$ = 682.1 nm) and (B) after ($\lambda_{max,1}$ = 430.5 nm and $\lambda_{max,2}$ = 705.2 nm) incubation in 1,6-hexanedithiol.

The maximum centered at ~680 nm arises from the in-plane polarization of the truncated tetrahedral nanoparticles. We note that the theoretically predicted LSPR maxima are ~70 nm red-shifted in comparison to the experimental results. This discrepancy arises from the slightly rounded triangular tips of the nanotriangles that are observed experimentally in Figure 1 compared to the sharp triangular tips used in the theoretical model.[42]

In previous work, we demonstrated that when 13 nm Au colloids are linked to surface confined Ag nanoparticles (using streptavidin linking between biotinylated nanoparticles), a red shift in the LSPR extinction maximum is observed.[21] Because all sides of the nanoparticles except for their bases are passivated in the stabilization process, it was hypothesized that the released nanoparticles could be asymmetrically functionalized. This could be achieved by incubating the nanoparticle samples in a passivating molecule while on the glass surfaces, then releasing the nanoparticles in a second solution that contains a functionally active molecule. Upon the addition of a linking agent, nanoparticle dimers could be formed. This could be achieved by biotinylating the nanoparticle bases and inducing dimer formation with streptavidin or by adding a dithiol such as 1,6-hexanedithiol to induce direct nanoparticle linking.

A simple model was used to demonstrate this principle. First, surface-confined nanoparticles were incubated in hexadecanethiol for ~72 h (as in the previous case). However, during the nanoparticle release step, ~2 μL of 1 mM 1,6-hexanedithiol was added during sonication (Figure 4A,B). As displayed in Figure 4, the addition of dithiol drastically influences the LSPR spectrum of the nanoparticles. Prior to dithiol addition, the LSPR spectrum reveals two distinct features: an intense peak at 417.9 nm and a weak, broad peak at 682.1 nm. Upon release of the nanoparticles in dithiol, the extinction maximum located at 417.9 nm shifts to 430.5 nm and decreases in intensity. Additionally, the local maximum located at 682.1 shifts to 705.2 nm and increases in intensity. To understand the nature of the extinction peaks, nanoparticle samples were analyzed structurally with TEM and theoretically with DDA.

To investigate the geometries of the linked nanoparticles, sample morphologies were characterized with TEM. As displayed in Figure 5A, the nanoparticle structures have changed dramatically, and no single triangular nanoparticles are observed. In fact, the shapes and contrast in these TEM images confirm the presence of nanoparticle dimers. Upon overlaying triangular frames onto the TEM image (Figure 5B), it appears that perfect nanoparticle dimers are not developing. Instead, slightly mismatched nanoparticle dimers are forming (Figure 5B). As

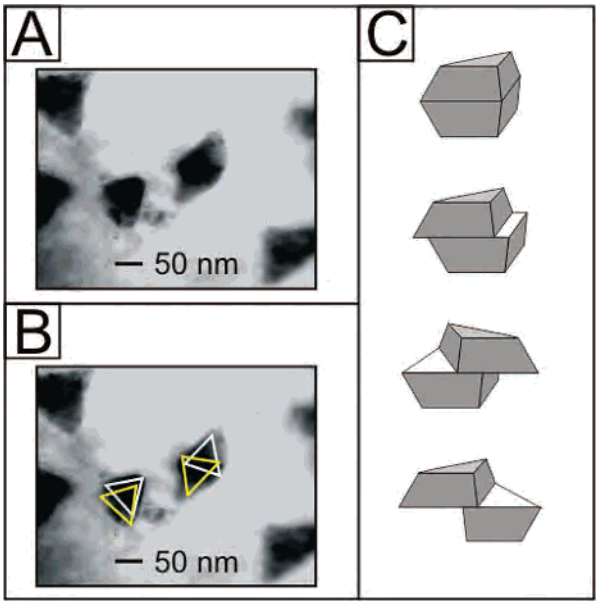

Figure 5. TEM characterization of nanoparticle dimers. (A and B) TEM reveals nanoparticles with various degrees of overlap (B contains triangular frames that help guide the eye for dimer formation). (C) Nanoparticle dimers overlap by varying degrees.

observed in Figure 5, the resulting dimers have perpendicular bisectors ranging from ~90 to 165 nm. It is hypothesized that the polycrystalline nature of the nanoparticles may be influencing the degree of overlap. If the nanoparticles were single crystals, the resulting dimer structures may well be different. To verify the observed degrees of overlap (Figure 5C) and to use them to understand the optical results of the nanoparticle dimers, DDA was used.

As in the previous case, DDA has been employed to model the nanoparticle dimers. Parameters and dipole grids were identical with those used previously. In the experimental spectrum in Figure 4B, the extinction maximum located at ~700 nm is relatively broad with a width of ~170 nm. It is hypothesized that the width of this peak arises from the combination of nanoparticle pairs with varying degrees of overlap. For this reason, the in-plane polarization extinction spectra have been calculated for dimers that have varying overlap between the two nanoparticles. Figure 6 shows that the extinction maxima span the range ~725 ± 30 nm for distances *d* (see the inset to Figure 6) in the range 15−25 nm. Although the spectral peak widths for a specific value of *d* are relatively narrow (~100 nm), a much larger (i.e. ~160 nm) overall peak width can be produced in the calculated results if a range of overlaps that is consistent with the TEM analysis is considered. This agrees well with the experimental width.

Conclusions

In conclusion, it has been demonstrated that a novel NSL method can be used to fabricate solution-phase triangular Ag nanoparticles. The results indicate that this technique can be used as a materials-general method to synthesize solution-phase nanoparticles inexpensively, uniformly, and precisely, and with size-tunable dimensions. In addition, this technique enables the asymmetric functionalization of Ag nanoparticles with self-assembled monolayers, and the subsequent release of these nanoparticles by sonication. Structural characterization with TEM revealed the presence of isolated triangles in the released sample, along with small spherical fragments. Upon repeating these experiments in the presence of a linking agent (dithiol),

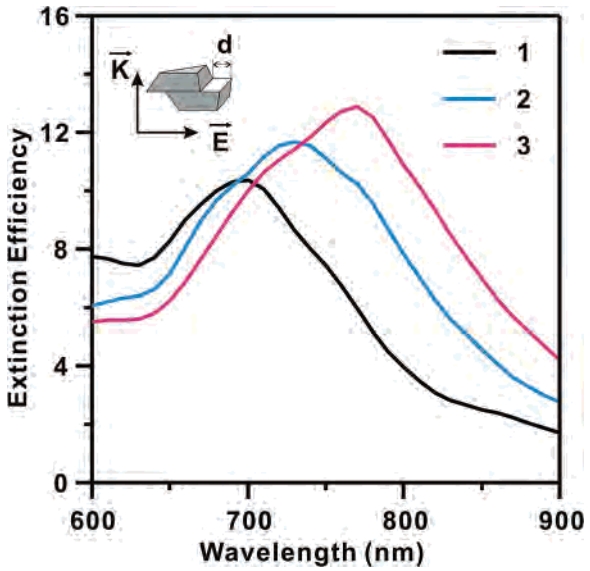

Figure 6. Theoretical calculations for nanoparticle dimers. DDA calculation of extinction spectra of a pair of linked Ag nanoparticles ($a = 95$ nm, $b = 50$ nm) with a SAM shell of hexadecanethiol in a bulk ethanol environment. The degree of nonoverlap d between the two bases of the Ag nanotriangles is (A) 15, (B) 20, and (C) 25 nm.

nanoparticle dimers were observed. The optical properties of the released Ag nanoparticles have been monitored with UV−vis extinction spectroscopy, and simulated with Mie theory and the Discrete Dipole Approximation method. Future spectroscopic investigations of these released single nanoparticles and their dimers will include nonensembled averaged characterization with single particle scattering spectroscopy, which should provide a better understanding of their optical spectra. Once the optical response of these structures is more thoroughly controlled, nanoparticle dimer formation can be used to detect a small number of sandwiched biological targets.

Acknowledgment. The authors gratefully acknowledge support from the National Science Foundation (EEC-0118025, CHE-0414554) and the Air Force Office of Scientific Research MURI program (Grant F49620-02-1-0381). Any opinions, findings, and conclusions or recommendations expressed in this paper are those of the authors and do not necessarily reflect those of the National Science Foundation.

References and Notes

(1) Haynes, C. L.; Van Duyne, R. P. *J. Phys. Chem. B* **2001**, *105*, 5599.
(2) Mulvaney, P. *MRS Bull.* **2001**, *26*, 1009.
(3) El-Sayed, M. A. *Acc. Chem. Res.* **2001**, *34*, 257.
(4) Link, S.; El-Sayed, M. A. *J. Phys. Chem. B* **1999**, *103*, 8410.
(5) Kreibig, U.; Gartz, M.; Hilger, A.; Hovel, H. Optical investigations of surfaces and interfaces of metal clusters. In *Advances in Metal and Semiconductor Clusters*; Duncan, M. A., Ed.; JAI Press Inc. (Stamford): New York, 1998; Vol. 4, p 345.
(6) Mulvaney, P. *Langmuir* **1996**, *12*, 788.
(7) Kreibig, U. Optics of nanosized metals. In *Handbook of Optical Properties*; Hummel, R. E., Wissmann, P., Eds.; CRC Press: Boca Raton, FL, 1997; Vol. II, p 145.
(8) Kreibig, U.; Gartz, M.; Hilger, A. *Ber. Bunsen-Ges.* **1997**, *101*, 1593.
(9) Jensen, T. R.; Kelly, K. L.; Lazarides, A.; Schatz, G. C. *J. Cluster Sci.* **1999**, *10*, 295.
(10) Freeman, R. G.; Grabar, K. C.; Allison, K. J.; Bright, R. M.; Davis, J. A.; Guthrie, A. P.; Hommer, M. B.; Jackson, M. A.; Smith, P. C.; Walter, D. G.; Natan, M. J. *Science* **1995**, *267*, 1629.
(11) Kahl, M.; Voges, E.; Kostrewa, S.; Viets, C.; Hill, W. *Sens. Actuators, B* **1998**, *51*, 285.
(12) Schatz, G. C.; Van Duyne, R. P. *Electromagnetic Mechanism of Surface-Enhanced Spectroscopy*; Wiley: New York, 2002; Vol. 1.
(13) Haynes, C. L.; Van Duyne, R. P. *J. Phys. Chem. B* **2003**, *107*, 7426.
(14) Haynes, C. L.; McFarland, A. D.; Zhao, L.; Van Duyne, R. P.; Schatz, G. C.; Gunnarsson, L.; Prikulis, J.; Kasemo, B.; Käll, M. *J. Phys. Chem. B* **2003**, *107*, 7337.
(15) Dirix, Y.; Bastiaansen, C.; Caseri, W.; Smith, P. *Adv. Mater.* **1999**, *11*, 223.
(16) Haynes, C. L.; Van Duyne, R. P. *Nano Lett.* **2003**, *3*, 939.
(17) Maier, S. A.; Brongersma, M. L.; Kik, P. G.; Meltzer, S.; Requicha, A. A. G.; Atwater, H. A. *Adv. Mater.* **2001**, *13*, 1501.
(18) Maier, S. A.; Kik, P. G.; Atwater, H. A.; Meltzer, S.; Harel, E.; Koel, B. E.; Requicha, A. A. G. *Nat. Mater.* **2003**, *2*, 229.
(19) Shelby, R. A.; Smith, D. R.; Schultz, S. *Science* (*Washington, DC*) **2001**, *292*, 77.
(20) Andersen, P. C.; Rowlen, K. L. *Appl. Spectrosc.* **2002**, *56*, 124A.
(21) Haes, A. J.; Van Duyne, R. P. *J. Am. Chem. Soc.* **2002**, *124*, 10596
(22) Mucic, R. C.; Storhoff, J. J.; Mirkin, C. A.; Letsinger, R. L. *J. Am. Chem. Soc.* **1998**, *120*, 12674.
(23) Hirsch, L. R.; Jackson, J. B.; Lee, A.; Halas, N. J.; West, J. L. *Anal. Chem.* **2003**, *75*, 2377.
(24) Haes, A. J.; Van Duyne, R. P. *Mater. Res. Soc. Symp. Proc.* **2002**, *723*, O3.1.1.
(25) Haes, A. J.; Van Duyne, R. P. *Laser Focus World* **2003**, *39*, 153.
(26) Haes, A. J.; Van Duyne, R. P. *SPIE* **2003**, *5221*, 47.
(27) Haes, A. J.; Zou, S.; Schatz, G. C.; Van Duyne, R. P. *J. Phys. Chem. B* **2004**, *108*, 6961.
(28) Haes, A. J.; Zou, S.; Schatz, G. C.; Van Duyne, R. P. *J. Phys. Chem. B* **2004**, *108*, 109.
(29) Riboh, J. C.; Haes, A. J.; McFarland, A. D.; Yonzon, C. R.; Van Duyne, R. P. *J. Phys. Chem. B* **2003**, *107*, 1772.
(30) Fritzsche, W.; Taton, T. A. *Nanotechnology* **2003**, *14*, R63.
(31) Aizpurua, J.; Hanarp, P.; Sutherland, D. S.; Kall, M.; Bryant, G. W.; Garcia de Abajo, F. J. *Phys. Rev. Lett.* **2003**, *90*, 057401/1.
(32) Obare, S. O.; Hollowell, R. E.; Murphy, C. J. *Langmuir* **2002**, *18*, 10407.
(33) Nath, N.; Chilkoti, A. *Proc. SPIE−Int. Soc. Opt. Eng.* **2002**, *4626*, 441.
(34) Nam, J.-M.; Thaxton, C. S.; Mirkin, C. A. *Science* (*Washington, DC*) **2003**, *301*, 1884.
(35) Bailey, R. C.; Nam, J.-M.; Mirkin, C. A.; Hupp, J. T. *J. Am. Chem. Soc.* **2003**, *125*, 13541.
(36) Lee, P. C.; Meisel, D. *J. Phys. Chem.* **1982**, *86*, 3391.
(37) Frens, G. *Nature Phys. Sci* **1973**, *241*, 20.
(38) Jana, N. R.; Gearheart, L.; Murphy, C. J. *J. Phys. Chem. B* **2001**, *105*, 4065.
(39) Murphy, C. J.; Jana, N. R. *Adv. Mater.* **2002**, *14*, 80.
(40) Kim, S. R.; Abbott, N. L. *Langmuir* **2002**, *18*, 5269.
(41) Sun, Y.; Mayers, B.; Herricks, T.; Xia, Y. *Nano Lett.* **2003**, *3*, 955.
(42) Jin, R.; Cao, Y. W.; Mirkin, C. A.; Kelly, K. L.; Schatz, G. C.; Zheng, J. G. *Science* **2001**, *294*, 1901.
(43) Jin, R.; Cao, Y. C.; Hao, E.; Metraux, G. S.; Schatz, G. C.; Mirkin, C. A. *Nature* (*London, UK*) **2003**, *425*, 487.
(44) Maillard, M.; Giorgio, S.; Pileni, M. P. *J. Phys. Chem. B* **2003**, *107*, 2466.
(45) Maillard, M.; Giorgio, S.; Pileni, M. P. *Adv. Mater.* **2002**, *14*, 1084.
(46) Hao, E. C.; Kelly, K. L.; Hupp, J. T.; Schatz, G. C. *J. Am. Chem. Soc.* **2002**, *124*, 15182.
(47) Sun, Y. G.; Xia, Y. N. *Science* **2002**, *298*, 2176.
(48) Hao, E.; Bailey, R. C.; Schatz, G. C.; Hupp, J. T.; Li, S. Y. *Nano Lett.* **2004**, *4*, 327.
(49) Yun, M. H.; Myung, N. V.; Vasquez, R. P.; Lee, C. S.; Menke, E.; Penner, R. M. *Nano Lett.* **2004**, *4*, 419.
(50) Walter, E. C.; Zach, M. P.; Favier, F.; Murray, B. J.; Inazu, K.; Hemminger, J. C.; Penner, R. M. *ChemPhysChem* **2003**, *4*, 131.
(51) Penner, R. M. *J. Electroanal. Chem.* **2002**, *522*, 1.
(52) Kohli, P.; Wirtz, M.; Martin, C. R. *Electroanalysis* **2004**, *16*, 9.
(53) Martin, C. R.; Mitchell, D. T. Template-synthesized nanomaterials in electrochemistry. In *Electroanalytical Chemistry*; Marcel Dekker: New York, 1999; Vol. 21, p 1.
(54) Hulteen, J. C.; Van Duyne, R. P. *J. Vac. Sci. Technol. A* **1995**, *13*, 1553.
(55) Hulteen, J. C.; Treichel, D. A.; Smith, M. T.; Duval, M. L.; Jensen, T. R.; Van Duyne, R. P. *J. Phys. Chem. B* **1999**, *103*, 3854.
(56) Dimitrov, A. S.; Nagayama, K. *Langmuir* **1996**, *12*, 1303.
(57) Mie, G. *Ann. Phys.* (*Weinheim, Germany*) **1908**, *25*, 377.
(58) Huffman, C. F. B. a. D. R. *Absorption and Scattering of Light by Small Particles*; Wiley-Interscience: New York, 1983.
(59) Draine, B. T.; Flatau, P. J. *J. Op. Soc. Am. A* **1994**, *11*, 1491.
(60) Kelly, K. L.; Coronado, E.; Zhao, L.; Schatz, G. C. *J. Phys. Chem. B* **2003**, *107*, 668.
(61) Lynch, D. W.; Hunter, W. R. In *Handbook of Optical Constants of Solids*; Palik, E. D., Ed.; Academic Press: New York, 1985; p 350.